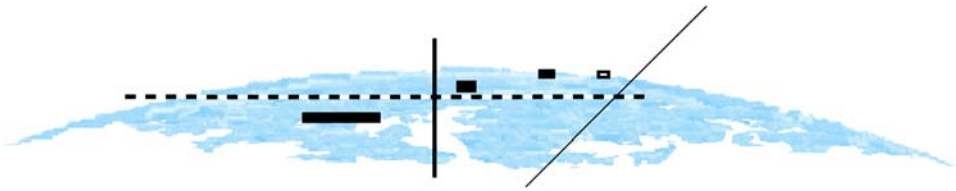

GeoForschungsZentrum Potsdam

STIFTUNG DES ÖFFENTLICHEN RECHTS

Scientific Technical Report

Continuation of the Earth's magnetic field into a core layer with differential rotation

H. Greiner-Mai[1], L. Ballani[2], D. Stromeyer[3]

GeoForschungsZentrum Potsdam (GFZ), Telegrafenberg, D-14473 Potsdam, Germany

[1,2] Division 1: Kinematics & Dynamics of the Earth
e-mail: [1]grm@gfz-potsdam.de, [2]bal@gfz-potsdam.de
[3] Division 5: Geomechanics & Geotechnology
e-mail: stro@gfz-potsdam.de

Continuation of the Earth's magnetic field into a core layer with differential rotation

H. Greiner-Mai[1], L. Ballani[2], D. Stromeyer[3]

GeoForschungsZentrum Potsdam (GFZ), Telegrafenberg, D-14473 Potsdam, Germany; [1,2] Division 1: Kinematics & Dynamics of the Earth, e-mail: [1]grm@gfz-potsdam.de, [2]bal@gfz-potsdam.de, [3] Division 5: Geomechanics & Geotechnology, e-mail: stro@gfz-potsdam.de

Summary

In a previous paper, we have calculated the poloidal magnetic field at the core-mantle boundary (CMB) from the Gauss coefficients of the geomagnetic field at the Earth surface. The numerical solution of the mantle induction equation is based on a modified Tikhonov regularization of an integral equation approach. We have tested the method for several conductivity models of the mantle and a passive upper-core layer.

This paper deals with the inverse solution of the induction equation accounting for *moving* core material. In a layer of the fluid outer core we prescribe the associated velocity field by a differential rotation in the outer core, the angular velocity of which near the CMB corresponds to the mean westward drift of the geomagnetic field. Apart from the conventional applications of the frozen-field theory, we solve the complete induction equation for the poloidal magnetic field in the mantle as well as in the fluid outer core layer using the magnetic field as boundary values at the Earth's surface and the assumed velocity field as prescribed model parameter.

This numerical experiment shows both the scope of our method with respect to highly conducting material and the effect of the motion of the conducting material on the penetration behavior of field variations.

The results indicate that the field continuation by our method is possible down to about 100 km below the CMB in the decadal time scale. The penetration depth mainly depends on the high conductivity while the effect of the relative rotation is marginal in the uppermost 25 km and becomes more significant in deeper parts. For depths of the outer core below 100 km, the solution procedure becomes more unstable and no relevant solution, fitting the data within 10%, can be reached, i.e., decadal field variations at

these depths cannot be fully causally related to those observed at the Earth's surface.

Key words: internal magnetic field, induction equation, inverse problem, core rotation, downward continuation

1 Introduction

For several problems of core dynamics, the geomagnetic field and its variation must be known in the core-mantle-boundary (CMB) region. Such problems are, e.g., the electromagnetic (EM) core-mantle-coupling and the determination of the velocity field $\mathbf{v}$ of the liquid core. At present, there is no comprehensive theoretical framework for determining the structure and material parameters in the CMB region. Recent investigations suggest that the CMB region is a complex transition zone including several kilometers of the upper core and a few hundred kilometers of the lower-most mantle (e.g., Buffett, 1992; Lay et al., 1998).

Although the findings about the structure of the CMB region are preliminary and partially controversial, we assume that a highly conducting shell may exist and must be taken into account in studies of core-mantle interactions, like the EM coupling and angular momentum exchange between core and mantle. An example is the determination of the velocity field of the core in the CMB region by inverting the frozen-field equation in the case where the CMB is covered on the core side by a non-moving layer of core material. The radial component of the magnetic flux then has to be determined not at the CMB but at the inner boundary of this layer. Conventionally, approximative solutions of the induction equation (potential solutions, perturbation solutions) are applied if the electrical conductivity of the layer is much lower than that of the core, the time scale of variations is decadal larger and/or the thickness of the conducting layer is small. It is not the purpose of this paper to explore the scope of these methods for highly conducting parts of the CMB region and to define the corresponding parameter ranges, but to present and use an algorithm which solves, inversely, the induction equation more or less independently of the assumptions about these parameters, and is embedded in a comprehensive inversion technique.

Therefore, we have recently developed a method for the non-harmonic downward continuation of the geomagnetic field to the CMB for an electrically conducting mantle (Ballani et al., 1995, 1999, 2001). We solved the inverse boundary value problem associated with the EM induction equation by an adapted solution procedure based on the related, well developed theory of the inverse heat conduction equation (sometimes named the sideways heat equation) (Dinh Nho Hào and Gorenflo, 1991, Reinhardt and Seiffarth, 1993). To overcome the difficulties with a space-variable coefficient function in the differential equation, the solution algorithm uses an idea used in

geothermal inversion (Stromeyer 1983, 1984).

The induction equation for the poloidal geomagnetic field $\mathbf{B}_s$ was decomposed into decoupled differential equations of the second order for the harmonic (cosine and sine) modes $S_{nm}^{c,s}$ of the poloidal field scalar S defining the poloidal magnetic field by

$$\mathbf{B}_s = \text{curlcurl } (\mathbf{r}S). \tag{1}$$

The two boundary values are given by the Gauss coefficients of the geomagnetic potential field, g_{nm} and h_{nm}, at the Earth's surface, $r = R_E$, i.e., only on one side of the mantle approximated by an outer insulating shell ($R_\sigma \leq r \leq R_E$) and an inner electrically conducting shell ($R_c < r < R_\sigma$). Within the insulating shell, the magnetic field behaves like a potential field. Therefore, the boundary values are well known at $r = R_\sigma$. The mathematical problem of solving the induction equation for $r \in (R_c, R_\sigma)$, especially at R_c, is then an inverse problem which is severely ill-posed like the inverse heat conduction problem. We have recently treated this inverse boundary value problem for the induction equation in its equivalent form of a Volterra equation of the first kind (Eldén, 1995) and solved an regularizing optimal control problem for the unknown boundary function $f(t) = S_{nm}^{c,s}(R_c, t)$. An outline of this method is given in section 3.1 .

In this paper, we will enlarge this method to calculations of the magnetic field in a core shell in which the electrically conducting liquid rotates differentially with the angular velocity $\omega(r)$. The objective of this investigation is

1) to find and to test a numerical algorithm of the inverse solution of the induction equation for this moving core fluid with its prescribed velocity field and

2) to study the effect of the motion on the diffusion of magnetic field variations through the outer parts of the core.

The choice of a differential rotation is somewhat pragmatical: for the associated velocity field, $\mathbf{v} = \boldsymbol{\omega}\times\mathbf{r}$, $\boldsymbol{\omega} = (0, 0, \omega)$, the induction equation can be decomposed into two independent systems of differential equations for the poloidal and the toroidal magnetic field, respectively. This ensures that the poloidal magnetic field can be calculated without information about the toroidal field, $\mathbf{B}_t = \text{curl } (\mathbf{r}T)$. $\mathbf{B}_t$ is not considered here because further modeling and additional assumptions are necessary to calculate its boundary values at $r = R_c$.

The difference between the scalar differential equations valid only for the mantle, on one hand, and the mantle together with a core layer, on the other hand, is that the latter are coupled with respect to the sin- and cos-modes. The conductivity of the core is assumed to be constant but the velocity parameter $\omega(r)$ introduces an additional r dependent coefficient into the differential equations of the mantle-core induction equation. Therefore, these equations can not be solved independently and the algorithm applied up to now to the mantle induction equation must be modified for the inverse solution. Compared with the frozen-field theory, the terminology "inverse" is used here with respect to the determination of $\mathbf{B}_s$ and not of $\mathbf{v}$, which is a prescribed parameter function in this paper. Furthermore, in the frozen-field approximation, the diffusion term is conventionally neglected. For the inversion of the core induction equation with respect to $\mathbf{v}$ with the diffusion term considered, we refer to an approximation given by Gubbins (1996).

2. Induction equation of the core for an axially rotating fluid

In the following, we outline the derivation of the scalar induction equation given in textbooks, e.g. Krause and Rädler (1980). The vectorial induction equation of the core is given by

$$-\frac{1}{\mu_0\ \sigma_c}\ \mathrm{curl\ curl}\ \mathbf{B}\ +\ \mathrm{curl}\ (\mathbf{v}\times\mathbf{B})\ =\ \dot{\mathbf{B}},\quad \mathrm{div}\ \mathbf{B}\ =\ 0, \tag{2}$$

where μ_0 is the permeability of vacuum, σ_c is the constant electrical conductivity of the core, $\mathbf{B}$ is the magnetic flux density and $\mathbf{v}$ is the velocity field of moving core material. After decomposition of $\mathbf{B}$ into its poloidal and toroidal parts represented by scalar functions and of $\mathbf{v}\times\mathbf{B}$ according to

$$\mathbf{v}\times\mathbf{B}\ =\ \mathrm{curl}\ \mathbf{r}\ U\ +\ \mathbf{r}\ V\ +\ \mathrm{grad}\ W, \tag{3}$$

we obtain for the poloidal scalar S in eq. (1) the differential equation

$$\frac{1}{\mu_0\ \sigma_c}\Delta S\ +\ U\ =\ \dot{S}, \tag{4}$$

which only contains the scalar U of the toroidal part of $\mathbf{v}\times\mathbf{B}$ in eq. (3). This equation defines a representation of a vector field with non-vanishing divergence by three scalar functions, two of which are normed by $\oint ...\sin\vartheta \mathrm{d}\vartheta\mathrm{d}\varphi =$

0, like S and T. Applying the operator $\mathbf{r} \cdot$ curl to eq. (3), we obtain

$$\Omega U \;=\; -\,\mathbf{r}\ \mathrm{curl}\ (\mathbf{v} \times \mathbf{B}), \tag{5}$$

where Ω is the Laplacean at a sphere $r = \mathrm{const.}$,

$$\Omega \;=\; \frac{1}{\sin\,\vartheta}\frac{\partial}{\partial\vartheta}(\sin\,\vartheta\frac{\partial}{\partial\vartheta}) \;+\; \frac{1}{\sin^2\vartheta}\frac{\partial^2}{\partial\varphi^2}. \tag{6}$$

Using eqs.(1) and (5), we obtain, for a rotating fluid with $\mathbf{v} = \boldsymbol{\omega} \times \mathbf{r}$, the expression

$$\Omega U \;=\; -\,\boldsymbol{\omega}(r)\ (\mathbf{r} \times \mathrm{grad}\ \Omega S), \tag{7}$$

where $\boldsymbol{\omega}$ is the vector of the angular velocity. Eq. (7) is valid for an angular velocity $\boldsymbol{\omega}$ which is dependent on r. For the axisymmetric case, $\boldsymbol{\omega} = (0, 0, \omega(r))$, applied here, we obtain from eq. (7)

$$\Omega U \;=\; -\,(\frac{\partial \Omega S}{\partial\varphi}) \cdot \omega(r) \tag{8}$$

(see e.g. Krause and Rädler, 1980, p. 201).

Eq. (8) can be solved for the harmonic modes of U by using the spherical harmonic expansion of U and S, the Legendre's differential equation $\Omega Y_{nm} = -n(n+1)Y_{nm}$ for $Y_{nm} = P_{nm}(\cos\vartheta)\mathrm{e}^{im\varphi}$ and the normalization conditions of the spherical harmonic functions. By the spherical harmonic expansion of the poloidal scalar field,

$$S(r, \vartheta, \varphi, t) = \sum_{n,m}\ (S^c_{nm}(r,t)\cos m\varphi + S^s_{nm}(r,t)\sin m\varphi)\ \ P_{nm}(\cos\vartheta) \tag{9}$$

and of the scalar U in eq. (8), we obtain from the scalar induction equation (4) the following, in pairs coupled differential equations for the harmonic modes S^c_{nm}, S^s_{nm}

$$\frac{\partial^2 S^c_{nm}}{\partial r^2} + \frac{2}{r}\frac{\partial S^c_{nm}}{\partial r} - \frac{n(n+1)}{r^2}S^c_{nm} - \mu_0\ \sigma(r)\frac{\partial S^c_{nm}}{\partial t} - m\ \mu_0\ \sigma(r)\omega(r)S^s_{nm} = 0$$

$$\frac{\partial^2 S^s_{nm}}{\partial r^2} + \frac{2}{r}\frac{\partial S^s_{nm}}{\partial r} - \frac{n(n+1)}{r^2}S^s_{nm} - \mu_0\ \sigma(r)\frac{\partial S^s_{nm}}{\partial t} + m\ \mu_0\ \sigma(r)\omega(r)S^c_{nm} = 0$$

which can be written as

$$D_n\ S^{c[s]}_{nm}\ -[+]\ m\ \mu_0\ \sigma(r)\ \omega(r)\ S^{s[c]}_{nm}\ =\ 0, \tag{10}$$

using the operator

$$D_n \;=\; \frac{\partial^2}{\partial\, r^2} \;+\; \frac{2}{r}\frac{\partial}{\partial r} \;-\; \frac{n(n+1)}{r^2} \;-\; \mu_0\;\sigma(r)\;\frac{\partial}{\partial t}. \tag{11}$$

3 The algorithms for solving the induction equations

3.1 Inversion of the mantle induction equation

The equations of the harmonic modes of S in the conducting part of the mantle are obtained by choosing $\omega(r) = 0$ in eqs. (10) and replacing $\sigma(r)$ by the mantle conductivity $\sigma_M(r)$ in the operator (11). The resulting decoupled differential equations for the harmonic modes then read

$$\left[\frac{\partial^2}{\partial\, r^2} \;+\; \frac{2}{r}\frac{\partial}{\partial r} \;-\; \frac{n(n+1)}{r^2} \;-\; \mu_0\;\sigma_M(r)\;\frac{\partial}{\partial t}\right]\; u \;=\; 0, \tag{12}$$

where u stands for $S^{c,s}_{nm}$ (e.g., Ballani et al., 2001). The boundary conditions at the outer boundary of the conducting shell of the mantle, $r = R_\sigma$, are given by

$$u(R_\sigma, t) \;=\; \phi(t), \quad \frac{\partial u}{\partial r}(R_\sigma, t) + \frac{n+1}{R_\sigma} u(R_\sigma, t) \;=\; 0, \tag{13}$$

where $\phi(t)$ is inferred from the geomagnetic potential field at the Earth's surface by its continuation through an insulating shell to $r = R_\sigma$, corresponding to the conventional harmonic downward continuation $R_E \to R_\sigma$. The boundary function $\phi(t)$ is given by temporally discrete values of the Gauss coefficients g_{nm}, h_{nm} ("data") in a finite period, $0 \le t \le T$. The second of the boundary conditions (13) is a consequence of the well-known continuity of S and $\partial S/\partial r$, if a non-potential magnetic field within a conductor is continued by a potential field outside of it.

To solve the inverse boundary value problem for the unknown function $u(R_c, t)$, an initial condition,

$$u(r, 0) = \psi(r)\ , \quad R_c \le r \le R_\sigma \tag{14}$$

must be given. For the numerical calculations, we assume that $\psi(r)$ is the potential solution obtained for $\sigma_M = 0$, which corresponds to the stationary solution of eq. (12) ($\partial u/\partial t = 0$).

The algorithm for solving eq. (12) with the boundary conditions (13) is described by Ballani et al. (2001), from which we will give an outline below. In this preceding paper, we studied the inverse problem for the differential equations (12), (13) and (14) in the equivalent form of an integral equation of the first kind, which describes the linear relation between pure time functions for different r-levels: the unknown time function $f(t) = u(R_c, t)$ on R_c and the data function $\phi(t) = u(R_\sigma, t)$ on R_σ. This relation is represented by a Volterra integral equation

$$\phi(t) = \int_0^t k(t-\tau)\, f(\tau) d\tau, \tag{15}$$

if for the initial condition (14) $\psi(r) \equiv 0$. This condition is reached at the beginning of the algorithm by subtracting a suited stable boundary value problem. Obviously, the kernel $k(t)$ contains all the influence of r, R_σ, R_c, n, m and $\sigma(r)$. However, for $\sigma(r) \neq$ const., this function cannot longer be specified analytically. Thus, another method overcoming this deficiency has to be introduced: Eq.(15) represents a linear relationship $\phi = A\, f$, where A is an (abstract) linear operator, here the Volterra integral operator. With the decomposition of the unknown function f into base functions e_k, $f = \sum f_k\, e_k$, the formal relations

$$\phi \;=\; A\, f \;=\; A\,(\sum\; f_k\, e_k) = \sum\; f_k\, A\,(e_k) \tag{16}$$

can be written. As the term $A\,(e_k)$ means the solution of a stable two-side boundary value problem with the function $e_k(t)$ at R_c and the second boundary condition of (13) at R_σ (e.g., Cannon, 1984), a finite-dimensional matrix (a_{ik}), approximating the operator A, can be determined in the following way: A time discretization $\{t = t_i, i = 1, N\}$ is introduced and the base functions $e_k(t)$ are taken as the simplest form of the Kronecker tensor $e_k(t_i) = \delta_{ki}$. With the boundary conditions

$$\frac{\partial u^k}{\partial r}(R_\sigma, t) \;+\; \frac{n+1}{R_\sigma} u^k(R_\sigma, t) \;=\; 0, \quad u^k(R_c, t) = e_k(t)\;, \quad k = 1, \ldots, N, \tag{17}$$

the solution $u^k(r, t)$ of the two-side boundary value problem for the differential equation (12) can be calculated for each base function e_k. Since

$u^k = A\, e_k$, where e_k is a base function, it is clear that this solution forms the kth column of (a_{ik}), so that the whole matrix can be composed by its columns

$$(a_{ik}) := u^k(R_\sigma, t_i), \quad i = 1, \ldots, N, \quad k = 1, \ldots, N. \tag{18}$$

With the convolution kernel in eq. (15), the matrix (a_{ik}) has a Toeplitz structure. Thus, in practice it is only necessary to calculate the first matrix column ($k = 1$). The other columns ($k = 2, \ldots, N$) are then generated by shifting their elements downward iteratively, which results in the known triangular structure, i.e., the implementation of this step requires only the numerical solution of *one* stable boundary value problem.

Having the matrix (a_{ik}) determined, the regularization procedure can be started. We use a modified Tikhonov regularization (Hansen 1992, 1998), which accounts especially for the data error ϵ at R_σ. The unknown function $f(t) = u(R_c, t)$ is determined by the minimization

$$\min \|f\|_\beta \quad \text{subject to} \quad \|Af - \phi\|_\alpha \leq \epsilon. \tag{19}$$

While the second term in the procedure (19) controls the data approximation at R_σ, the first term searches for optimal smoothness of the solution at R_c. The norms are specified as the conventional L_2 norm for $\|.\|_\alpha$. The other one is chosen as W_2^1 norm.

The algorithm ends with a transform which restores the original initial condition.

3.2 Inversion of the mantle-core induction equation

The method for the inversion of the mantle induction equation outlined in section 3.1 can also be applied, with some modifications, to the corresponding inverse boundary value problem for eqs. (10), now including also the mantle and an outer-core layer. The two coupled equations (10) can be transformed into one complex equation, introducing the complex harmonic mode, $\tilde{u}$, by

$$\tilde{u} = S^c_{nm} + iS^s_{nm}, \qquad i = \sqrt{-1}\ . \tag{20}$$

From eqs. (10) we then obtain the complex differential equation for a particular complex mode

$$\tilde{D}_n \tilde{u} + i\ m\ \mu_0\ \sigma(r)\ \omega(r)\ \tilde{u}\ =\ 0, \tag{21}$$

which has a structure analogous to that of the mantle (eq. (12)), with the outer-core velocity $\omega(r)$ as an additionally assigned parameter function. Because we are now interested to solve the inverse problem for time functions $\tilde{u}(R_{oc}, t), R_{oc} < R_c$, on a r-level beneath the CMB in the fluid outer core, the range of r-values is enlarged to the interval $[R_{oc}, R_\sigma]$. The boundary values are taken, as above, only at the outer boundary R_σ, i.e., they remain exactly the same. Thus, the conditions (13) can be written in complex composed form as

$$\tilde{u}(R_\sigma, t) \;=\; \tilde{\phi}(t), \quad \frac{\partial \tilde{u}}{\partial r}(R_\sigma, t) + \frac{n+1}{R_\sigma}\tilde{u}(R_\sigma, t) \;=\; 0. \tag{22}$$

The choice of an initial condition needs additional consideration. For the mantle, the used harmonic downward continuation, condition (14), $\sigma_M = 0$, corresponds to the stationary solution of eqs. (12). This principle is kept also for the core: The initial value function $\tilde{\psi}(r) = \tilde{u}(r, 0), R_{oc} \le r \le R_\sigma$, is determined numerically in advance from a system of ordinary differential equations which is obtained from eq. (21) by neglecting the time derivative terms. (For comparison, this solution is also shown in the figures denoted by "steady-state" in the next section.)

The solution algorithm of the mantle-core inverse boundary value problems can be applied by full analogy as described in section 3.1: The relations (16) can be understood in complex form. The solutions $\tilde{u}^k$ of the stable two-side boundary value problems (17) are generated with the complex base functions $\tilde{e}_k(t) = \tilde{e}_k^{Re}(t) + \; i\; \tilde{e}_k^{Im}(t)$ at the lower boundary R_{oc} and the second complex outer boundary condition given at R_σ (22). From $\tilde{u}^k$, the complex matrix $(\tilde{a}_{ik}) = \tilde{u}^k(R_\sigma, t_i)$ for the regularization procedure (19) can be derived. The regularized solution of the inverse problem $\tilde{u}(R_{oc}, t) = S_{nm}^c(R_{oc}, t) + iS_{nm}^s(R_{oc}, t)$ contains the harmonic modes $S_{nm}^{c,s}(R_{oc}, t)$ as its real part and imaginary part, respectively.

4 Model assumptions: Data, conductivity and velocity models

The data used are the Gauss coefficients given by Bloxham and Jackson (1992). On the basis of a spline interpolation, they are taken equally spaced ($\Delta t = 2$ years) covering the time interval 1690–1990. As an example, we demonstrate the downward continuation for the [1,1] and [5,5] harmonic

modes. Hereafter, we do not introduce new notations for the harmonic coefficients at different radii (different depth beneath the CMB), but keep for simplicity the original notations. From the pairs g_{ij}, h_{ij} only the g_{11} and g_{55} components will be presented and discussed here.

The assumed conductivity model is given by

$$\sigma(r) = \begin{cases} 0 & R_\sigma < r \\ 10 * (\frac{R_c}{r})^5 & R_c + 200 \text{ km} < r \leq R_\sigma \\ 3000 & R_c \leq r \leq R_c + 200 \text{ km} \\ 2 * 10^5 & R_c > r, \end{cases} \tag{23}$$

where the unit of $\sigma(r)$ is Sm^{-1} and the basic radii are taken as $R_\sigma = 5480$ km and $R_c = 3485$ km. For the region in the interval $R_c + 200$ km $< r \leq R_\sigma$, the mantle conductivity is chosen according to the results in laboratories (e.g., Shankland et al., 1993). The effect of this shell on the inverse solution is marginal in the decadal time scale. For the lower-most shell of the mantle (e.g., the D" layer), we assume that the conductivity model is consistent with the conductance necessary for the EM core-mantle coupling and decadal length-of-day variations (Holme, 1998). This is valid for our model (23), but can also be reached by other combinations of the thickness of the shell and the value of σ_M. Besides this, the assumed model (23) should be considered primarily as an example for which the numerical algorithm will be demonstrated.

For the value of the velocity function $\omega(r)$ at the CMB ($r = R_c$), we choose the mean westward drift of the outer core, $\omega_c = -0.1^\circ\,\mathrm{a}^{-1}$ (e.g., Greiner-Mai, 1986). Further, we prescribe the radial dependence of ω for $r \in (R_c - 100 \text{ km}, R_c)$ by the alternative possibilities a) a step function and b) a continuous increase to zero, both shown in Fig. 1. The model assumptions about $\omega(r)$ imply that the observed variations (except a global westward drift) are caused by processes (sources of the secular variation) in core parts lying deeper than the respective R_{oc} value.

We choose a maximum depth of 100 km, because the skin depth is about 20 to 60 km for periods of 20 to 100 years and we expect that the solution becomes unstable for $r < R_c - 100$ km. The results are then compared with the inverse solutions for the stationary case and a non-moving layer ($\omega = 0$, denoted as "model 0" hereafter). The potential solution is obtained if both $\omega = 0$ and the stationary case are chosen.

The models of relative rotation are shown in Fig. 1. The Figs. 2-3 show the

resulting variations of the poloidal g_{11}, g_{55} modes at several radii, $R_{oc} \leq R_c$, as an example.

5 Results

In the following, we will discuss i) the influence of the model of mantle conductivity, ii) the influence of the relative rotation of the core and its conductivity and iii) the differences between the non-stationary and the stationary solutions in the core.

i) The upper curves in Fig. 2 show the "data" at the Earth surface, i.e., the values of the Gauss coefficients g_{11} and g_{55}; the lower curves show the associated CMB values derived by non-harmonic downward continuation as "model 0". The curves can be compared with the steady-state solution, which corresponds to the potential solution ("model 0 (steady state)"). However, according to the primary objective of this paper, we will study the field behavior in the outer parts of the core and refer to further discussions of the influence of the mantle conductivity $\sigma_M(r)$ by Ballani et al. (2001). Compared with the field variations obtained for the core (Fig. 3), the differences between the potential solution and the inverse solution for the conducting mantle at the CMB are rather marginal, although they are significant with respect to the EM core-mantle coupling.

ii) With respect to the core, the results for model 0 ($\omega = 0$) show the absolute effect of the high conductivity in the core on the variations of the poloidal modes. Comparing with those for the other ω models, we conclude that the penetration behavior is dominated by the high conductivity. As shown in Fig. 3, the influence of the relative rotation is rather weak in the first 25 km below the CMB [in Fig. 3 a), the differences between the models 1 and 2 are so small that they could not be displayed], but it becomes more significant for $r = R_c - 50$ km and deeper parts. The figs. 3 b) and c) show that the differences between the models 1 and 2 become significantly larger in deeper parts of the core. The graphs for g_{11} show that the relative rotation amplifies the values of this coefficient compared to that with zero-velocity. Furthermore, this amplification is stronger for model 2, which suggests that the different directions of the relative rotation in model 1 ($\omega < 0$ in $r \in (R_c - 25$ km) versus $\omega > 0$ in $r \in (R_c - 50$ km)) cause a partial cancellation of the effect of the relative rotation. However, this cannot clearly be concluded

from the behavior of g_{55}.

iii) The departures from the steady-state solutions are significant at all levels of r, R_{oc} and become large at the deepest shell considered. As expected, the phase shift between the stationary and the non-stationary solutions increases with depth and reaches values of about 40 years for $r = R_c - 100$ km. Comparing the variations for the different ω models, we can conclude that the phase shifts and the increase of their amplitudes are the major effects of the relative rotation, whereas the spectral content of the variations is not changed. As expected from the governing equations, the spectral content will be changed if ω is assumed to be time dependent.

In addition, Fig. 3 c) shows large oscillations of g_{55}. The first part of the time interval is dominated by the influence of the required initial condition by which a certain arbitrariness is introduced. As a measure of its length, the phase shift can be considered, which amounts to about 40 years for $r = R_c - 100$ km. Therefore, the irregular behavior in, e.g., Fig. 3 c) for g_{55} in the first 40 years is a typical effect of the regularization procedure. The large amplitudes of the variations in the middle of the curves indicate that the algorithm approaches numerical instability. To this subject, it must be mentioned that the misfit bound, $\epsilon_m = \|\phi(.) - u(R_\sigma, .)\|$, at R_σ (see procedure (19)) is chosen as 5% for $r \geq R_c - 50$ km, corresponding to the assumed error level of the data. This r level is then the maximum depth for which no instabilities appear. For $r = R_c - 100$ km, we need a higher ϵ_m value (10 %) to reach a stable solution, otherwise the solution becomes unstable for $\epsilon_m = 5\%$ and $r = R_c - 100$ km, corresponding to the typical trade-off in the Tikhonov regularization. From a physical point of view, this behaviour may be associated with crossing the skin depth of decadal variations by downward continuation. Because we are not dealing with single frequencies, this skin depth cannot be quantified by only one value of r and is an interval of radii according to the frequency spectrum of the used time series. The associated effects in the numerical method are the instability and an r dependent ϵ_m necessary to reach stable solutions.

Nevertheless, some tens of kilometers below $r = R_c - 100$ km stability can no more be reached by reasonable ϵ_m values, i.e., solutions of physical relevance can no longer be determined for depths greater 100 km, by this method.

6 Conclusions

We show that the algorithm, by which we solved the inverse mantle-induction problem recently (Ballani et. al., 2001), can be enlarged to the outermost core with small modifications if the velocity field of the outer core is approximated with a relative differential rotation. As the method does not represent a kind of disturbance theory but provides the full inversion free from assumptions on the scale of the magnetic field, it is able to account for the high conducting core material at least down to a depth of 100 km combined with the prescribed motions. Nevertheless, for a more realistic velocity field, the situation will be more complicated, in particular if the toroidal field must be considered. Therefore, our investigation should only be understood as a preliminary step in the investigation of the inverse induction problem of the core.

By an example calculation we show that the effect of the high conductivity dominates the downward continuation. The influence of the relative rotation is marginal in the first 25 km of the outer core and becomes more significant in deeper parts. The comparison with the stationary solution shows that the inverse solution is stable in the first 50 km of the upper core if a data error ϵ_m of 5% at $r = R_\sigma$ is allowed; for 100 km depth, this value must be increased to 10% in order to at all construct a reasonable solution. Besides possible physical constraints not considered in this paper, this behaviour is probably related to an r dependent skin effect appearing if the boundary values are given by a discrete finite time series with a certain spectral band instead of a single harmonic signal.

The method used can be applied to calculations of geomagnetic variations in the outer core necessary for investigations of the velocity field by frozen-flux theory, calculations of EM torques and estimates of the strength of the magnetic-flux in the outer-core parts. The pure induction effects (e.g., in a passive layer) are known; a further physical interpretation of these problems compared with conventional approximative solutions should be explored in the near future.

Acknowledgment

We thank our colleague Dr. Richard Holme for helping us with the ufm data models and some associated programs. Furthermore, we thank Prof. Rutger Wahlstrøm of the University Uppsala (presently staying at the GFZ) for his valuable hints leading to a more understandable presentation.

7 References

Ballani, L., Greiner-Mai, H. and Stromeyer, D., 1995. Über ein nicht-charakteristisches Cauchy-Problem bei der geomagnetischen Kern-Mantel-Kopplung., Z. Angew. Math. Mechanik, ZAMM, 75: 613-614.

Ballani, L., Greiner-Mai, H. and Stromeyer, D., 1999. Determining the magnetic field in the Earth's deep mantle by an inverse boundary value problem. Sci. Tech. Rep. GFZ Potsdam STR99/12, 52 pp.

Ballani, L., Greiner-Mai, H. and Stromeyer, D., 2001. Determining the magnetic field in the core-mantle-boundary zone by non-harmonic downward continuation. submitted to Geophys. J. Int.

Bloxham, J. and Jackson, A., 1992. Time-dependent mapping of the magnetic field at the core-mantle boundary, J. Geophys. Res., 97: 19,537-19,563.

Buffett, B. A., 1992. Constraints on magnetic energy and mantle conductivity from the forced nutations of the Earth. J. Geophys. Res., 97: 19,5681-19,597.

Cannon, J.R., 1984. The One-Dimensional Heat Equation, Addison-Wesley, Reading, MA.

Dinh Nho Hào, and Gorenflo, R., 1991. A noncharacteristic Cauchy problem for the heat equation. Acta Appl. Math. 24: 1-27.

Eldén, L., 1995. Numerical Solution of the Sideways Heat Equation. in: Inverse Problems in Diffusion Processes, H. Engl and W. Rundell, eds., Philadelphia, SIAM, pp. 130-150.

Greiner-Mai, H., 1986. Westward drift of the Earth's core and the Earth's rotation. Gerlands Beitr. Geophysik, 95: 341-354.

Gubbins, D. 1996. A formalism for the inversion of geomagnetic data for core motions with diffusion. Phys. Earth Planet. Inter., 98: 193-206.

Hansen, P. C., 1992, 1998. Regularization Tools. A Matlab Package for Analysis and Solution of Discrete Ill-Posed Problems, Lyngby, Denmark, 109 pp.

Holme, R., 1998. Electromagnetic core-mantle coupling - II. Probing deep mantle conductance. The Core-Mantle Boundary Region. in: M. Gurnis, M. E. Wysession, E. Knittle and B. A. Buffett, eds., The Core-Mantle Boundary Region, American Geophysical Union, Washington, pp. 139-151.

Krause, F. and Rädler, K. H., 1980. Mean Field Magnetohydrodynamics and Dynamo Theory. Akademie Verlag, Berlin.

Lay, T., Williams, Q. and Garnero, E. J., 1998. The core-mantle boundary layer and deep Earth dynamics. Nature, 392: 461-468.

Reinhardt, H.-J. and Seiffarth, F., 1993. On the Approximate Solution of Illposed Cauchy Problems for Parabolic Differential Equations. In: Anger, G., et al., eds., Inverse Problems: Principles and Applications in Geophysics, Technology, and Medicine. Mathematical Research, Vol. 74., Akademie-Verlag, Berlin, pp. 284-298.

Shankland, T. J., Peyronneau, J. and Poirier, J.-P., 1993. Electrical conductivity of the Earth's lower mantle. Nature, 366: 453-455.

Stromeyer, D., 1983. Methodische Untersuchungen zur Inversion geothermischer Daten. Diss. Forschungsbereich Geo- und Kosmoswissenschaften, Akad. Wiss. d. DDR, Potsdam, 82 pp.

Stromeyer, D., 1984. Downward Continuation of Heat Flow Data by means of the Least Squares Method. Tectonophysics, 103: 55-66.

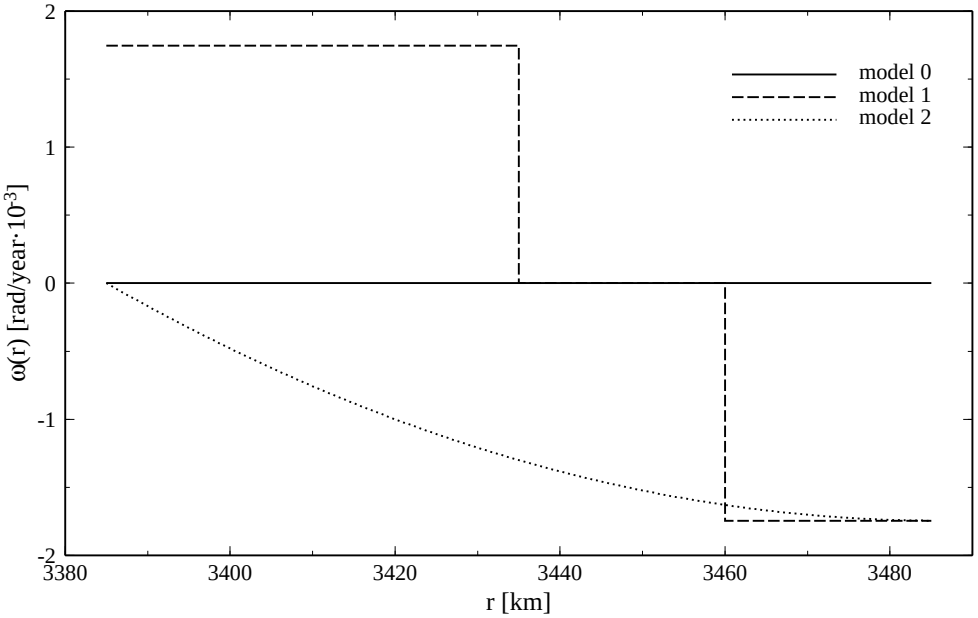

Figure 1: Prescribed dependence of the angular velocity, ω, on radius r

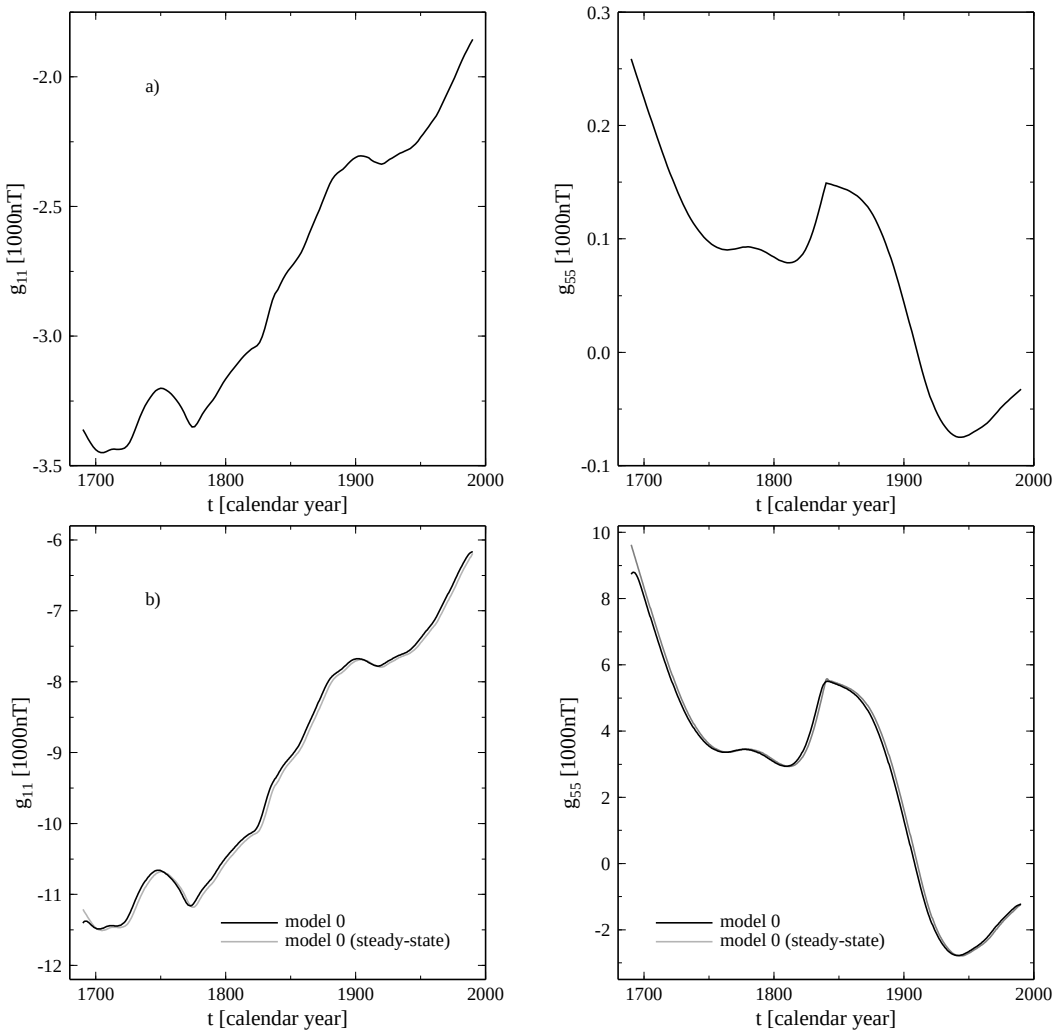

Figure 2: Spherical harmonic coefficients g_{11} and g_{55}: a) at the Earth's surface and b) downward continued to the CMB according to the conductivity model (23) of the mantle. They can be compared with the potential solution obtained for the "model 0 (steady-state)"

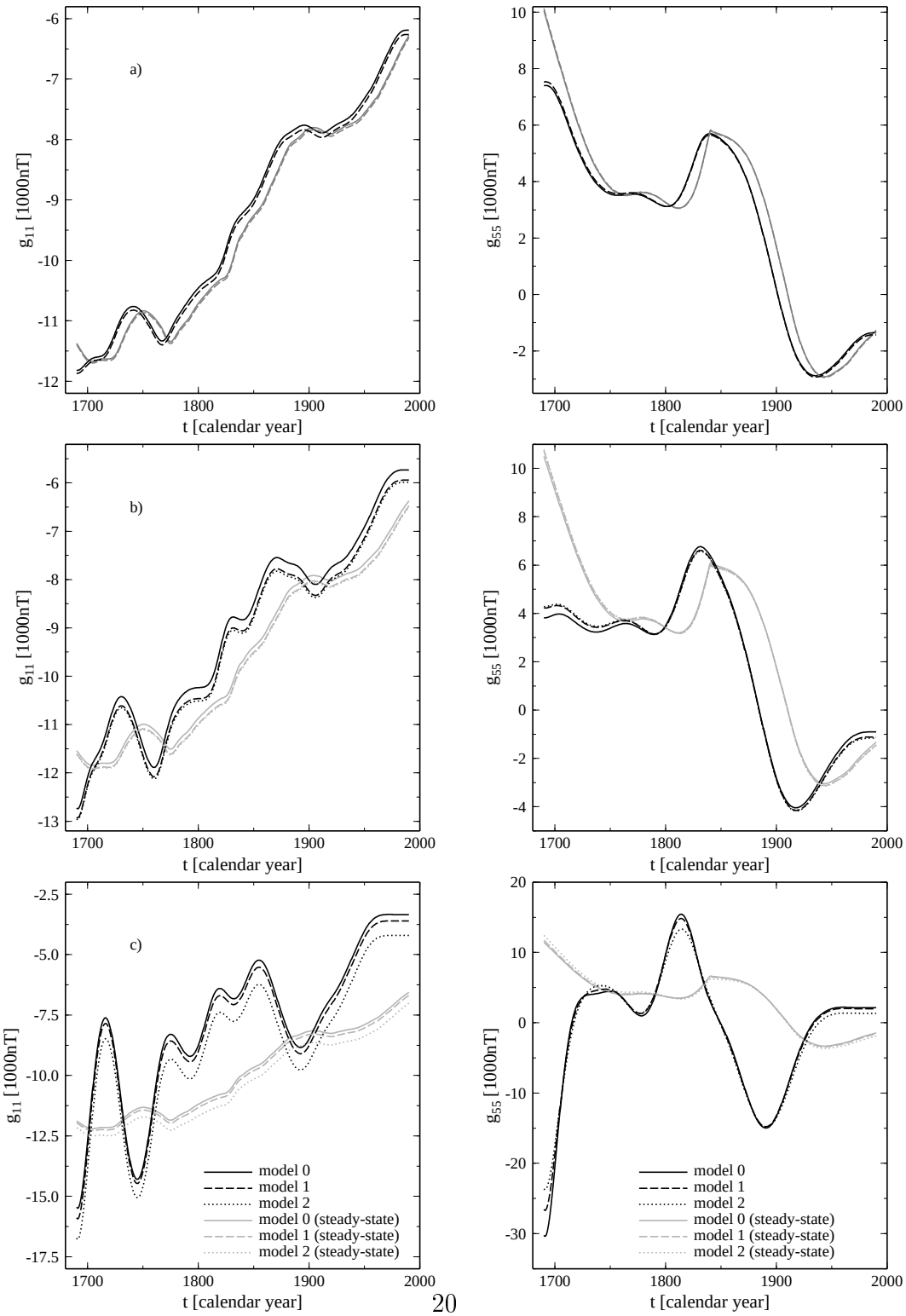

Figure 3: Spherical harmonic coefficients g_{11} and g_{55} continued to the spheres: a) $r = R_c - 25$ km, b) $r = R_c - 50$ km and c) $r = R_c - 100$ km inside the core for the models of the angular velocity, $\omega(r)$, shown in Fig. 1. Model 2 is not shown since in a) the difference to model 1 is insignificant.